Semivectorial polarised finite difference method for optical waveguides with arbitrary index profiles

M.S. Stern

Indexing terms: Waveguides and waveguide components, Dielectric materials

Abstract: A simple accurate method, which automatically takes full account of the discontinuities in the normal electric field components across any arbitrary distribution of internal dielectric interfaces, is presented for the determination of polarised solutions of the Helmholtz wave equation. The application of the shifted inverse power iteration method to the resulting matrices, enables any required propagation eigenvalue (not necessarily the fundamanetal mode) to be determined, together with its corresponding electric field profile. It is found that the results, which are presented for various semiconductor rib waveguide structures, compare favourably with published vector finite element and scalar results.

1 Introduction

Following recent developments in optoelectronics, there has been considerable interest in predicting the propagation modes of semiconductor rib (and channel) waveguides. A typical structure of such guides is shown in Fig. 1 (which also displays the directions of the axes assumed throughout this paper). The geometrical configuration, and the consequent piecewise constant refractive index profile $n(x, y)$, preclude analytical solutions of the Helmholtz wave equation. Furthermore, the complete solution of the electromagnetic field problem is vectorial, rather than scalar, in nature. There has been much activity devoted to obtaining approximate and numerical solutions of the scalar problem, with most of the attention being paid to variational and finite difference methods [1–5, 16]. More recently, vector $\boldsymbol{H}$ solutions have been obtained by means of finite difference [6, 7], finite element [8–14], and equivalent network [15] methods.

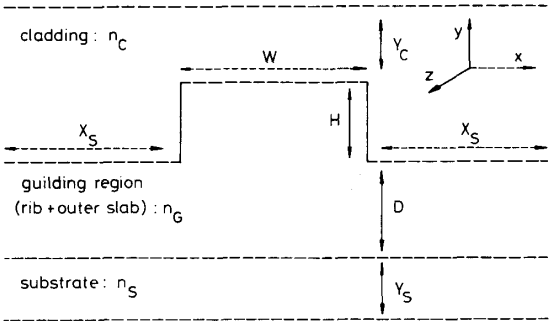

Fig. 1 *Typical semiconductor rib waveguide structure*
The refractive indices of the three regions are n_C, n_G, and n_S. The directions of the axes are also shown

In this paper, a semivectorial finite difference method is presented for determining polarised solutions of the Helmholtz equation in rib (or channel) waveguides, with arbitrary piecewise constant refractive index profiles. Quasi-TE and quasi-TM modes are represented, respectively, by the usual laboratory experimental horizontal and vertical polarisations, $(E_x, 0, E_z)$ and $(0, E_y, E_z)$, of the electric field $\boldsymbol{E}$. An analysis carried out in Section 2 shows that these polarisations lead to the decoupling of the component equations in the vector $\boldsymbol{E}$ Helmholtz wave equation, but to no decoupling of the components in the corresponding vector $\boldsymbol{H}$ equation. Quasi-TE modes are therefore eigensolutions of the scalar Helmholtz equation for the horizontal component E_x which is continuous across horizontal internal dielectric interfaces, but discontinuous across vertical interfaces, whilst quasi-TM modes are eigensolutions of the scalar Helmholtz equation for the vertical component E_y which is continuous across vertical interfaces, but discontinuous across horizontal interfaces. The longitudinal component E_z for either polarisation may then be computed from the appropriate transverse field component by means of a simple relationship between the two components. Under this approximation it is unnecessary to solve a pair of coupled scalar wave equations in order to determine the two non-zero components of either polarisation of the electric field. This approach does not seem to be valid for quasi-TE or TM solutions which start from the magnetic components.

In Appendix 8 it is shown how the Helmholtz equations for E_x and E_y can be approximated by different finite difference schemes which automatically take full account of the discontinuities in the normal electric field components across any arbitrary distribution of internal dielectric interfaces, provided that each interface is parallel to the x or y axis. Both schemes yield eigenvalue problems for different real non-symmetric band matrices.

Scalar modes may be determined by solving the Helmholtz equation for the component E_z which is parallel to all internal dielectric interfaces and is therefore continuous, with continuous first derivatives, throughout the solution domain. The usual five-point difference scheme is employed to approximate this wave equation, thus yielding an eigenvalue problem for a real symmetric band matrix. This is an alternative approach to the various methods used by other authors [1–5] to solve the scalar propagation problem for rib (or channel) waveguides.

Paper 5823J (E13), first received 9th June and in revised form 2nd October 1987

The author is with the Department of Applied and Computational Mathematics, University of Sheffield, Sheffield S10 2TN, United Kingdom

Full use is made of geometrical symmetry when setting up the finite difference matrices for the quasi-TE, quasi-TM, and scalar modes; a choice of outer boundary conditions is available. Only the non-zero band of any matrix is stored, with the grid being scanned in a way which minimises the band-width. The shifted inverse power iteration method [17] is employed to locate any required propagation eigenvalue (not necessarily the dominant one) and its corresponding electric field profile for the mode under investigation. Further information regarding the finite difference matrices and grid is contained in Section 3. Contrary to the suggestions made by Lagu and Ramaswamy [4], there is certainly no need to store complete square matrices (most of whose elements would be zero) and neither is there any need to carry out matrix inversions [16].

Various semiconductor rib waveguide structures are analysed in Section 4. Where comparisons are available, it is found that the semivectorial polarised finite difference method developed in this paper produces results which are in good agreement with published vector finite element [12] and scalar [3, 5] results. The method is highly attractive owing to its accuracy and simplicity. It is certainly capable of generating results which compare very favourably with those produced by a vector $\boldsymbol{H}$ finite element analysis of optical waveguide structures.

2 Theory

For harmonic wave propagation in the z direction along a rib (or channel) waveguide we consider the fields (in the usual notation)

$$\boldsymbol{E}(x, y, z, t) = (E_x, E_y, E_z) \exp j(\omega t - \beta z) \tag{1a}$$

$$\boldsymbol{H}(x, y, z, t) = (H_x, H_y, H_z) \exp j(\omega t - \beta z) \tag{1b}$$

$$\boldsymbol{D} = \varepsilon(x, y)\boldsymbol{E}, \quad \boldsymbol{B} = \mu \boldsymbol{H} \tag{2}$$

where the dielectric constant $\varepsilon(x, y)$ is piecewise constant and the magnetic permeability μ completely constant throughout the solution domain. The components of the electric and magnetic fields in eqn. 1 are functions of x and y only. (The components of $\boldsymbol{B}$ and $\boldsymbol{D}$ may be similarly defined.) Then, from Maxwell's equations (for source-free regions), namely,

$$\nabla \cdot \boldsymbol{D} = 0, \quad \nabla \cdot \boldsymbol{B} = 0 \tag{3a}$$

$$\nabla \times \boldsymbol{E} = -\partial \boldsymbol{B}/\partial t = -j\omega\mu \boldsymbol{H} \tag{3b}$$

$$\nabla \times \boldsymbol{H} = \partial \boldsymbol{D}/\partial t = j\omega\varepsilon \boldsymbol{E} \tag{3c}$$

we obtain

$$\nabla \times (\nabla \times \boldsymbol{E}) = \nabla(\nabla \cdot \boldsymbol{E}) - \nabla^2 \boldsymbol{E} = \omega^2 \varepsilon\mu \boldsymbol{E} = k^2 \boldsymbol{E} \tag{4}$$

in which

$$k(x, y) = \omega(\varepsilon\mu)^{1/2} = 2\pi n(x, y)/\lambda \tag{5}$$

where λ is the free space wavelength. By taking the divergence of both sides of eqn. 4 we find that

$$\nabla \cdot \boldsymbol{E} = -\boldsymbol{E} \cdot \nabla \log_e k^2 \tag{6}$$

which may be substituted into eqn. 4 to yield the wave equation

$$\nabla^2 \boldsymbol{E} + k^2 \boldsymbol{E} + \nabla(\boldsymbol{E} \cdot \nabla \log_e k^2) = 0 \tag{7}$$

As $k(x, y)$ is piecewise constant,

$$\nabla \log_e k^2 = 0$$

and it should also be noted that $\nabla \log_e k^2$ is undefined at internal dielectric interfaces where $k(x, y)$ is discontinuous. Hence, by observing that eqn. 1 gives the identities

$$\partial/\partial z \equiv j\beta, \quad \partial^2/\partial z^2 \equiv -\beta^2$$

we find that eqn. 7 reduces to the Helmholtz wave equation

$$\nabla_T^2 \boldsymbol{E} + k^2 \boldsymbol{E} = \beta^2 \boldsymbol{E} \tag{8}$$

in which $\nabla_T^2 = \partial^2/\partial x^2 + \partial^2/\partial y^2$.

We now proceed by considering the three component equations of eqn. 8. The treatment of scalar modes is briefly dealt with in subsection *2.1* below. For quasi-TE and quasi-TM modes, respectively considered in subsections *2.2* and *2.3* below, we use a semivectorial approach suggested by laboratory experiments where it is widely assumed, and well verified in practice (although it does not appear to be documented), that the two polarisations E_x and E_y tend to persist unchanged over thousands of wavelengths. This suggests that our present approach is midway between the scalar and vector theories, and we have described our approach as 'semivectorial'.

2.1 Scalar modes

Scalar modes (which are equivalent to the scalar solutions presented by other authors [1–5]) we solve the equation

$$\nabla_T^2 E_z + k^2 E_z = \beta^2 E_z \tag{9}$$

As E_z, $\partial E_z/\partial x$, and $\partial E_z/\partial y$ are continuous throughout the solution domain, the usual five-point difference scheme (see Appendix 8) is employed to convert eqn. 9 into the algebraic eigenvalue problem

$$A_S \boldsymbol{E}_S = \beta_S^2 \boldsymbol{E}_S \tag{10}$$

in which A_S is a real symmetric band matrix, β_S^2 is the scalar mode propagation eigenvalue, and $\boldsymbol{E}_S$ is the corresponding normalised eigenvector representing the field profile $E_z(x, y)$.

2.2 Quasi-TE modes

For quasi-TE modes we consider the laboratory polarisation

$$\boldsymbol{E} \equiv (E_x, 0, E_z) \exp j(\omega t - \beta z) \tag{11}$$

and then find that Maxwell's equations (eqns. 3) yield

$$\partial E_x/\partial x = j\beta E_z, \quad \partial E_x/\partial y = j\omega B_z, \quad \partial E_z/\partial y = -j\omega B_x \tag{12}$$

Continuity of E_z, B_z, and B_x across horizontal and vertical dielectric interfaces implies that $\partial E_x/\partial x$, $\partial E_x/\partial y$, and $\partial E_z/\partial y$ are continuous across the same interfaces. Thus, quasi-TE modes are the eigensolutions of the equation

$$\nabla_T^2 E_x + k^2 E_x = \beta^2 E_x \tag{13}$$

with E_x continuous across horizontal interfaces but discontinuous across vertical interfaces. The component $E_z(x, y)$ may then be determined from the first of the relations (eqn. 12). Appendix 8 contains the derivation of a finite difference scheme which automatically takes full account of the discontinuity in E_x across any vertical interface, and yields the algebraic eigenvalue problem

$$A_{TE} \boldsymbol{E}_{TE} = \beta_{TE}^2 \boldsymbol{E}_{TE} \tag{14}$$

in which A_{TE} is a real non symmetric band matrix, β_{TE}^2 is the TE propagation eigenvalue, and $\boldsymbol{E}_{TE}$ is the corresponding normalised eigenvector representing the field profile $E_x(x, y)$.

2.3 Quasi-TM modes

For quasi-TM modes we consider the laboratory polarisation

$$\boldsymbol{E} \equiv (0, E_y, E_z) \exp j(\omega t - \beta_z) \tag{15}$$

and then observe that Maxwell's equations (eqn. 3) yield the relations

$$\partial E_y/\partial y = j\beta E_z, \quad \partial E_y/\partial x = -j\omega B_z, \quad \partial E_z/\partial x = j\omega B_y \tag{16}$$

Continuity of E_z, B_z, and B_y across horizontal and vertical interfaces leads to the continuity of $\partial E_y/\partial y$, $\partial E_y/\partial x$, and $\partial E_z/\partial x$ across these interfaces. Hence, quasi-TM modes are the eigensolutions of the equation

$$\nabla_T^2 E_y + k^2 E_y = \beta^2 E_y \tag{17}$$

with E_y continuous across vertical interfaces, but discontinuous across horizontal interfaces. The component E_z may then be found from the first of the relations (eqn. 16). Appendix 8 contains a brief derivation of a finite difference scheme which automatically takes full account of the discontinuity in E_y across any horizontal interface and leads to the algebraic eigenvalue problem

$$A_{TM}\boldsymbol{E}_{TM} = \beta_{TM}^2 \boldsymbol{E}_{TM} \tag{18}$$

where A_{TM} is a real non-symmetric band matrix ($\neq A_{TE}$ in general), β_{TM}^2 is the TM propagation eigenvalue, and $\boldsymbol{E}_{TM}$ is the corresponding normalised eigenvector for the field profile $E_y(x, y)$.

2.4 Quasi-TE and Quasi-TM modes

We observe that, for both quasi-TE and quasi-TM modes, eqns. 3*a* and *c*, respectively, yield

$$\partial H_x/\partial x + \partial H_y/\partial y = j\beta H_z \tag{19}$$

$$(1/\varepsilon)(\partial H_y/\partial x - \partial H_x/\partial y) = j\omega E_z \tag{20}$$

As H_z and E_z are continuous across horizontal and vertical dielectric interfaces, it follows that the expressions on the LHS's of eqns. 19 and 20 must also be continuous across the same interfaces. (However, this does not imply continuity of each derivative of H_x and H_y.) Furthermore, it can be established from (3*c*) that $\partial H_z/\partial x$ and $\partial H_z/\partial y$ are continuous across horizontal and vertical interfaces for both quasi-TE and quasi-TM modes. Hence all three components of the magnetic field $\boldsymbol{H}$ are always present, in contrast to the experimental polarisations $(E_x, 0, E_z)$ and $(0, E_y, E_z)$ of the electric field $\boldsymbol{E}$. This means that the three component equations of the magnetic Helmholtz wave equation

$$\nabla_T^2 \boldsymbol{H} + k^2 \boldsymbol{H} = \beta^2 \boldsymbol{H} \tag{21}$$

must always be solved simultaneously for both quasi-TE and quasi-TM modes, in contrast to the procedure that may be employed for polarised solutions of eqn. 8.

3 Finite difference matrices

Each of the eigenvalue problems (eqns. 10, 14, and 18) is solved by means of the shifted inverse power iteration method [17, 18] (coupled with LU factorisation of the shifted matrix) which enables any required range of propagation eigenvalues to be determined together with their corresponding normalised electric field profiles. Each eigenvector is normalised so that its component of largest magnitude is equal to unity.

When setting up any of the finite difference schemes described in Appendix 8, each internal interface is placed half-way between adjacent grid lines. The grid points are separated by constant step lengths h_x and h_y in the horizontal and vertical directions, respectively. Each internal grid point is situated at the centre of a rectangular cell of constant refractive index; changes in refractive index are allowed to occur only at cell boundaries (see Fig. 2). The

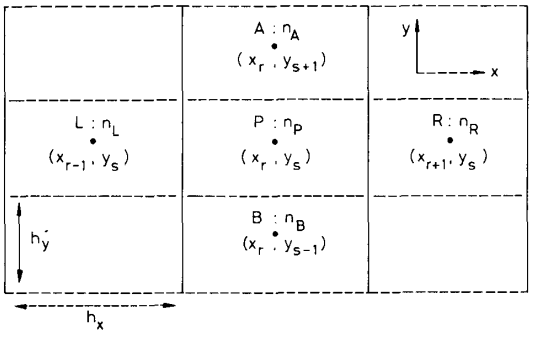

Fig. 2 *Cell structure of the finite difference grid*

The centre co-ordinates and constant refractive index of each cell involved in forming a five-point difference approximation at the point (x_r, y_s) are shown. Changes in refractive index occur only at cell boundaries. Each cell has sides of length h_x and h_y

finite difference grid is scanned in a way which minimises the band-widths of the matrices A_S, A_{TE}, and A_{TM}, with only the non-zero band of any matrix being stored. The three finite difference schemes can easily handle, without modification, waveguide geometries which are more complicated than those shown in Fig. 1, provided that each interface is parallel to the x or y axis.

Full use is made of geometrical symmetry when setting up the matrices A_S, A_{TE}, and A_{TM}. For rib waveguides of the form illustrated in Fig. 1, it is only necessary to solve eqns. 9, 13 and 17 on the right-hand (or left-hand) half of the structure. For even (symmetrical) modes $\partial E_x/\partial x$, $\partial E_y/\partial x$, and $\partial E_z/\partial x$ are set to zero along the vertical symmetry axis, whilst for odd (asymmetric) modes the field values themselves are set to zero along this axis. The finite difference grid lies within a rectangular box. On the outer boundary of this box it is usual to apply either

(*a*) a closed boundary condition of zero field values at all points provided the box is sufficiently large, or

(*b*) an open boundary condition of exponential decay of field values in directions normal to the horizontal and vertical sides of the box

Obviously, the size of the box containing the grid is less critical for condition (*b*) than for (*a*). However, when the mode to be determined is close to cut-off, the box size must be sufficiently large for both conditions (*a*) and (*b*) in order to allow for the substantial field penetration into the substrate. It should be noted that condition (*b*) is equivalent to the use of infinite elements by Rahman and Davies [9, 12] in their vector finite element (VFE) method. As the exponential decay constant is $(\beta^2 - k^2)^{1/2}$, condition (*b*) requires correction through a set of outer iterations superimposed over the (inner) inverse power iterations. This involves updating the value of β used in the decay constant at the end of each cycle of inner iterations. Such a cycle forms one outer iteration for correcting the decay constant.

After determining any modal eigenvalue β^2 of a rib (or other) waveguide it is useful to calculate the effective

eigenvalue

$$\beta_{eff}^2 = (\beta/k_0)^2 \quad \text{where} \quad k_0 = 2\pi/\lambda \tag{22}$$

and the normalised index (which indicates how far a mode is from cut-off)

$$b = (\beta_{eff}^2 - n_S^2)/(n_G^2 - n_S^2) \tag{23}$$

(see Fig. 1. for notation).

4 Results

The method established in Sections 2 and 3, and in Appendix 8 has been employed, with considerable success, to investigate propagation modes of various dielectric rib waveguide structures. We first examine the application of the method to the three structures analysed by Robertson *et al.* [3]. The optical and geometrical parameters of these structures (called BT1, BT2, and BT3) are given in Table 1, whilst values of β_{eff} and b for the dominant even scalar, quasi-TE, and quasi-TM modes appear, respectively, in Tables 2A, 2B, and 2C. It can be seen clearly that the scalar results of Table 2A are in close agreement with values presented in Reference 3, but there are no comparisons available for the polarised results of Tables 2B and 2C. It is observed that the choice of outer boundary condition does not affect the computed values of β_{eff} and b for the strongly guiding structure BT1, but that it does produce changes (in the expected direction) for the weaker guiding structures BT2 and BT3. Contour and surface plots of the fundamental TE field within each structure (with exponential decay on the outer box boundary) are presented in Figs. 3*a*, 3*b*, 4*a*, 4*b*, 5*a*, and 5*b*.

We now turn our attention to two of the structures (called UCL1 and UCL2 in this paper) analysed by Rahman and Davies [12] with their vector finite element (VFE) method. Their optical and geometrical parameters appear in Tables 3 and 4. Dominant even mode results, as a function of the outer slab thickness D (and rib height H), are presented in Tables 5*a* and *b* for UCL1, together with available VFE values [5, 12] for comparison. It is observed that for $D < 0.7$ μm ($H > 0.3$ μm), the scalar and quasi-TE results are, respectively, almost equally slightly above and slightly below the corresponding VFE-TE values. For 0.7 μm $\leqslant D \leqslant 1.0$ μm ($H \leqslant 0.3$ μm) both scalar and quasi-TE values lie a little above their VFE-TE counterparts. In fact, for most values of the outer slab thickness, the quasi-TE and scalar results presented here are closer to the corresponding VFE-TE values than the scalar comparisons quoted in Reference 5. No comparisons are available for the quasi-TM results displayed in Table 5*a* and *b*.

Contour and surface plots of the leading assymetrical TE field within UCL1, with $D = H = 0.5$ μm, are displayed in Figs. 6*a* and 6*b*. This mode is not far above cut-off, with $b = 0.0652$. Further solutions of eqn. 14 have established that cut-off for assymetrical TE modes (with $\lambda = 1.15$ μm) occurs when the outer slab thickness of UCL1 falls below 0.4 μm.

Tables 6*a* and *b* contain polarised values of β_{eff} and b, as a function of substrate depth, for the multimode rib waveguide structure UCL2. The dominant, even TM results are in excellent agreement with the H_{11}^x plot of b displayed in Fig. 8*b* of reference 12 whilst the leading odd TE values are close to the H_{11}^y plot of b presented in Fig. 7*b* of reference 12. The values of b displayed in Fig. 7*b* of reference 12 may be incorrectly labelled.

Table 1: The semiconductor rib waveguide structures of reference 3 (see Figs. 1 and 2 for notation). The wavelength considered was $\lambda = 1.55$ μm

Structure	n_G	n_S	n_C	W μm	H μm	D μm	X_S μm	Y_S μm	Y_C μm	h_x μm	h_y μm
BT1	3.44	3.34	1.0	2	1.1	0.2	3.00	5.025	0.525	0.0952	0.05
BT2	3.44	3.36	1.0	3	0.1	0.9	3.05	5.025	0.525	0.0968	0.05
BT3	3.44	3.435	1.0	4	2.5	3.5	4.34	7.550	0.550	0.0976	0.10

Table 2A: Dominant, even scalar modes for the rib waveguide structures of Reference 3 and Table 1 ($\lambda = 1.55$ μm)

Boundary condition	Zero field on the outer box boundary		Exponential decay on the outer box boundary	
Structure	β_{eff}	b	β_{eff}	b
BT1	3.3901676	0.4979888	3.3901676	0.4979888
BT2	3.3954801	0.4406	3.3955255	0.4412
BT3	3.4367069	0.3412	3.4368442	0.3687

Table 2B: Dominant, even quasi-TE modes for the rib waveguide structures of Reference 3 and Table 1 ($\lambda = 1.55$ μm)

Boundary condition	Zero field on the outer box boundary		Exponential decay on the outer box boundary	
Structure	β_{eff}	b	β_{eff}	b
BT1	3.3869266	0.4655926	3.3869266	0.4655926
BT2	3.3953942	0.4395	3.3954405	0.4401
BT3	3.4366674	0.3333	3.4368112	0.3621

Table 2C: Dominant, even quasi-TM modes for the rib waveguide structures of Reference 3 and Table 1 ($\lambda = 1.55$ μm)

Boundary condition	Zero field on the outer box boundary		Exponential decay on the outer box boundary	
Structure	β_{eff}	b	β_{eff}	b
BT1	3.3867447	0.4637752	3.3867447	0.4637751
BT2	3.3905538	0.3792	3.3905927	0.3796
BT3	3.4366376	0.3274	3.4367719	0.3542

5 Conclusion

In this paper a simple accurate finite difference method has been presented for determining polarised $\boldsymbol{E}$ field solutions of the Helmholtz wave equation. The finite difference schemes for the quasi-TE and quasi-TM modes automatically take full account of the discontinuities in the appropriate normal electric field components across any arbitrary distribution of internal dielectric interfaces. Where comparisons are available it has been found that this semivectorial approach, which is justified by the theoretical analysis of Section 2, yields results which compare very favourably with those produced by a vector $\boldsymbol{H}$ finite element analysis, but without the complexity of the latter.

The theory and method of analysis developed in Sections 2 and 3 and Appendix 8 have been validated indirectly by curvature loss calculations. Computed values of β^2 and of the corresponding electric field profiles have been used in a curvature loss formula presented in references 19 and 20; the resulting theoretical loss values have been found to be in good agreement with those measured experimentally [19].

The semivectorial polarised finite difference method is currently being employed to determine propagation modes of directional couplers, channel waveguides, and of structures with more layers than shown in Fig. 1.

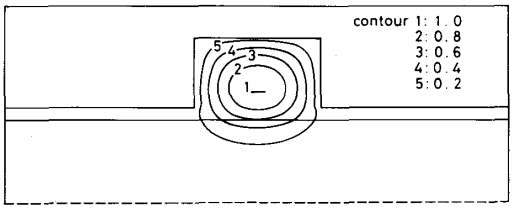

Fig. 3a *Fundamental TE field within the structure BT1 of reference 3 and Table 1*

Contour levels are at 20% intervals of the maximum field. (λ = 1.55 μm)
contour 1—1.0
2—0.8
3—0.6
4—0.4
5—0.2

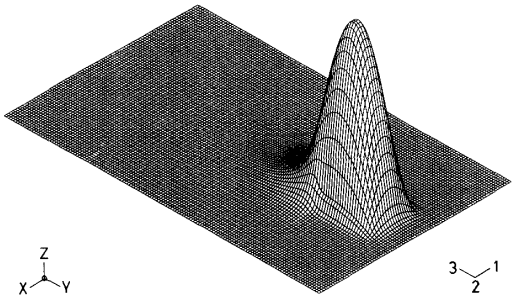

Fig. 3b *Fundamental TE field within the structure BT1 of Reference 3 and Table 1*

(λ = 1.55 μm)

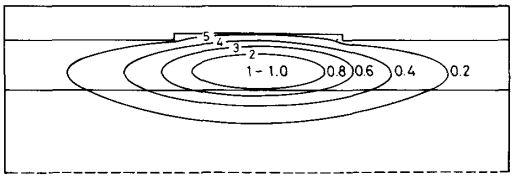

Fig. 4a *Fundamental TE field within the structure BT2 of Reference 3 and Table 1*

Contour levels are at 20% intervals of the maximum field. (λ = 1.55 μm)

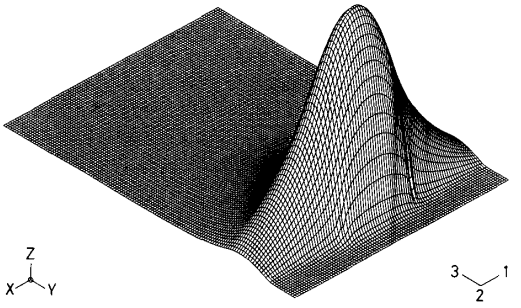

Fig. 4b *Fundamental TE field within the structure BT2 of Reference 3 and Table 1*

(λ = 1.55 μm)

6 Acknowledgments

The author is very grateful to Prof. P.C. Kendall for many interesting and fruitful discussions. Thanks are also due to Dr. R.C. Hewson-Browne for helpful comments.

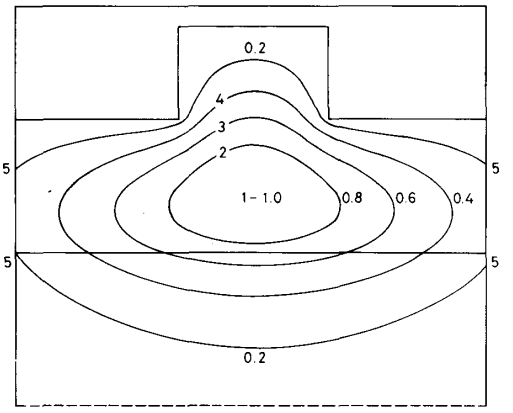

Fig. 5a *Fundamental TE field within the structure BT3 of Reference 3 and Table 1*

Contour levels are at 20% intervals of the maximum field. (λ = 1.55 μm)

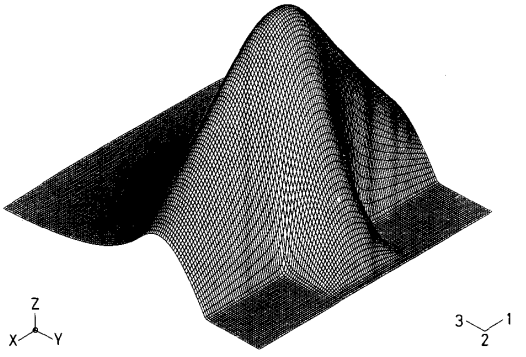

Fig. 5b *Fundamental TE field within the structure BT3 of Reference 3 and Table 1*

(λ = 1.55 μm)

Table 3: A semiconductor rib waveguide structure (UCL1) from reference 12 (see Figs. 1 and 2 for notation). The wavelength considered was λ = 1.15 μm

n_G	n_S	n_C	W μm	$H+D$ μm	X_S μm	Y_S μm	Y_C μm	b_x μm	h_y μm
3.44	3.40	1.00	3	1	2.952	5.025	1.025	0.0968	0.05

Table 4: A semiconductor rib waveguide structure (UCL2) from reference 12. (See Figs. 1 and 2 for notation). The wavelength considered was λ = 1.15 μm

n_G	n_S	n_C	W μm	H μm	D μm	X_S μm	Y_C μm	h_x μm	h_y μm
3.4406	3.4145	1.00	14	0.5	1.0	3.056	1.025	0.197	0.05

7 References

1 BENSON, T.M.: 'Integrated optical components produced in GaAs and InP epitaxial layers using the photo-elastic affect', Ph.D thesis, Dept. of Electronic and Electrical Engineering, University of Sheffield, 1982

Table 5a: Dominant, even mode values of β_{eff} for the structure UCL1 of Reference 12 and Table 3. VFE results from References 5 and 12 are given for comparison ($\lambda = 1.15$ μm). (The discrepancy between the VFE-TE and quasi-TE results may, of course, be due to curve reading errors from Reference 12).

D μm	Ref. 12 VFE-TE	Semi-vectorial method		
		Scalar	Quasi-TE	Quasi-TM
0.0	3.4121	3.41233	3.41188	3.41051
0.1	3.4122	3.41243	3.41200	3.41060
0.2	3.41235	3.41257	3.41217	3.41073
0.3	3.41255	3.41277	3.41240	3.41092
0.4	3.41285	3.41303	3.41271	3.41117
0.5	3.41315	3.41337	3.41310	3.41150
0.6	3.41365	3.41379	3.41358	3.41190
0.7	3.4141	3.41431	3.41415	3.41241
0.8	3.41475	3.41493	3.41484	3.41303
0.9	3.4156	3.41571	3.41568	3.41385
1.0	3.4171	3.41733	3.41733	3.41551

Table 5b: Dominant even mode values of b for the structure UCL1 of Reference 12 and Table 3. VFE results from References 5, 12 are given for comparison ($\lambda = 1.15$ μm) (The discrepancy between the VFE-TE and quasi-TE results may, of course, be due to curve reading errors from Reference 12)

D μm	Ref. 12 VFE-TE	Semi-vectorial method		
		Scalar	Quasi-TE	Quasi-TM
0.0	0.2988	0.3071	0.2959	0.2617
0.1	0.3038	0.3094	0.2987	0.2639
0.2	0.3075	0.3129	0.3029	0.2672
0.3	0.3125	0.3179	0.3088	0.2718
0.4	0.3200	0.3245	0.3165	0.2780
0.5	0.3275	0.3330	0.3263	0.2862
0.6	0.3399	0.3436	0.3382	0.2964
0.7	0.3512	0.3563	0.3525	0.3089
0.8	0.3674	0.3719	0.3696	0.3245
0.9	0.3886	0.3914	0.3905	0.3448
1.0	0.4261	0.4319	0.4319	0.3863

2 AUSTIN, M.W.: 'Theoretical and experimental investigation of GaAs/GaAlAs and nn GaAs rib waveguides', *IEEE J. Lightwave Technol.*, 1984, **2,** pp. 688–694

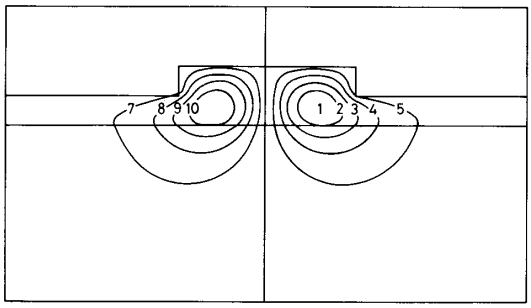

Fig. 6a *Leading asymmetric TE field within the structure UCL1 of Reference 12 and Table 3, with $D = H = 0.5$ μm*

Contour levels are at 20% intervals of the maximum field. ($\lambda = 1.15$ μm, $\beta_{eff} = 3.40262$, $b = 0.0652$)

contour 1—1.0 6— 0.0
2—0.8 7— −0.2
3—0.6 8— −0.4
4—0.4 9— −0.6
5—0.2 10— −0.8

3 ROBERTSON, M.J., RITCHIE, S., and DAYAN, P.: 'Semiconductor waveguides: analysis of optical propagation in single rib structures and directional couplers', *IEE Proc. J.*, 1985, **132,** pp. 336–342

4 LAGU, R.K., and RAMASWAMY, R.V.: 'A variational finite difference method for analysing channel waveguides with arbitrary index profiles', *IEEE J. Qunatum Electron.*, 1986, **22,** pp. 968–976

5 KENDALL, P.C., ADAMS, M.J., RITCHIE, S., and ROBERTSON, M.J.: 'A theory for calculating approximate values for propagation constants of an optical rib waveguide by weighting the refractive indices', *IEE Proc. A*, 1987, **134,** pp. 699.–702

6 SCHULZ, N., BIERWIRTH, K., and ARNDT, F.: 'Finite difference analysis of integrated optical waveguides without spurious mode solutions', *Electron. Lett.*, 1986, **22,** pp. 963–965

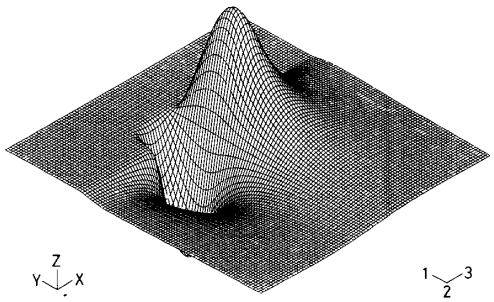

Fig. 6b *Leading asymmetric TE field within the structure UCL1 of Reference 12 and Table 3, with $D = H = 0.5$ μm*

($\lambda = 1.15$ μm, $\beta_{eff} = 3.40262$, $b = 0.0652$)

Table 6a: Dominant, even modes as a function of substrate depth for the structure UCL2 of Reference 12 and Table 4. The outer box boundary condition was exponential decay of field values ($\lambda = 1.15$ μm)

Y_s μm	Quasi-TE		Quasi-TM	
	β_{eff}	b	β_{eff}	b
0.525	3.42880	0.5468	3.42812	0.5208
1.025	3.42877	0.5459	3.42809	0.5198
1.525	3.42877	0.5457	3.42809	0.5196
2.025	3.42877	0.5457	3.42809	0.5196
2.525	3.42877	0.5457	3.42809	0.5196

Table 6b: Leading odd modes as a function of substrate depth for the structure UCL2 of Reference 12 and Table 4. The outer box boundary condition was exponential decay of field values ($\lambda = 1.15$ μm)

Y_s μm	Quasi-TE		Quasi-TM	
	β_{eff}	b	β_{eff}	b
0.525	3.42816	0.5226	3.42747	0.4962
1.025	3.42814	0.5218	3.42746	0.4958
1.525	3.42814	0.5215	3.42746	0.4957
2.025	3.42814	0.5215	3.42746	0.4957
2.525	3.42814	0.5215	3.42746	0.4957

7 BIERWIRTH, K., SCHULZ, N., and ARNDT, F.: 'Finite dfference analysis of rectangular dielectric waveguide structures', *IEEE Trans.*, 1986, **MTT-34,** pp. 1104–1114

8 MABAYA, N., LAGASSE, P.E., and VANDENBULCKE, P.: 'Finite element analysis of optical waveguides', *IEEE Trans.*, 1981, **MTT-29,** pp. 600–605

9 RAHMAN, B.M.A., and DAVIES, J.B.: 'Finite element analysis of optical and microwave waveguide problems', *IEEE Trans.*, 1984, **MTT-32,** pp. 20–28

10 RAHMAN, B.M.A., and DAVIES, J.B.: 'Finite element solution of optical waveguides', *IEEE J. Lightwave Technol.*, 1984, **2,** pp. 682–688

11 RAHMAN, B.M.A., and DAVIES, J.B.: 'Penalty function improvement of waveguide solution by finite elements', *IEEE Trans.*, 1984, **MTT-32,** pp. 922–928

12 RAHMAN, B.M.A., and DAVIES, J.B.: 'Vector-H finite element solution of GaAs/GaAlAs rib waveguides', *IEE Proc. J*, 1985, **132,** pp. 349–353

13 HAYATA, K., KOSHIBA, M., EGUCHI, M., and SUZUKI, M.: 'Novel finite element formulation without any spurious solutions for dielectric waveguides', *Electron Lett.*, 1986, **22,** pp. 295–296

14 YOUNG, T.P., and SMITH, P.: 'Finite element modelling of integrated optical waveguides', *GEC J. Research*, 1986, **4,** pp. 249–255

15 KOSHIBA, M., and SUZUKI, M.: 'Vectorial wave analysis of dielectric waveguides for optical integrated circuits using equivalent network approach', *IEEE J. Lightwave Technol.*, 1986, **4,** pp. 656–664

16 SCHWEIG, E., and BRIDGES, W.B.: 'Computer analysis of dielectric waveguides: a finite difference method', *IEEE Trans.*, 1984, **MTT-32,** pp. 531–541
17 WILKINSON, J.: 'The algebraic eigenvalue problem' (Clarendon Press, 1965)
18 JOHNSON, L.W., and RIESS, R.D.: 'Numerical analysis' (Addison-Wesley, 1977)
19 KENDALL, P.C., STERN, M.S., and ROBSON, P.N.: 'A Huygens-type formula for curvature loss from dielectric waveguides in optoelectronics', *Electron. Lett.*, 1987, **23,** pp. 850–851
20 KENDALL, P.C., STERN, M.S., and ROBSON, P.N.: 'A new curvature loss formula of Huygens type for rib waveguides', *IEE Proc. J*, 1988. **135,** (to be published)

8 Appendix

With reference to Fig. 2, finite difference schemes will be set up to approximate eqns. 9, 13 and 17 at any internal grid point (x_r, y_s).

8.1 Scalar modes

At (x_r, y_s) eqn. 9 may be replaced by the usual five point difference scheme

$$E_{r,s-1}/h_y^2 + E_{r-1,s}/h_x^2 + [k_{r,s}^2 - 2/h_x^2 - 2/h_y^2]E_{r,s} + E_{r+1,s}/h_x^2 + E_{r,s+1}/h_y^2 = \beta^2 E_{r,s} \quad \text{(A1)}$$

in which $k_{r,s} = k(x_r, y_s)$ and $E_{r,s} = E_z(x_r, y_s)$, etc. By applying this approximation at each internal grid point, with appropriate amendments when (x_r, y_s) is adjacent to the outer box boundary, we obtain the algebraic eigenvalue equation (eqn. 10).

8.2 Quasi-TE modes

At the interfaces between cells L and P and between cells P and R, the field component E_x satisfies the discontinuity conditions

$$\varepsilon_L E_{r-1/2,s}^{(L)} = \varepsilon_p E_{r-1/2,s}^{(P)}, \quad \varepsilon_p E_{r+1/2,s}^{(P)} = \varepsilon_R E_{r+1/2,s}^{(R)}$$

where $E_{r,s} = E_x(x_r, y_s)$, etc. In view of eqn. 5 these relationships may be rewritten as

$$k_{r-1,s}^2 E_{r-1/2,s}^{(L)} = k_{r,s}^2 E_{r-1/2,s}^{(P)} \quad \text{(A2}a\text{)}$$

$$k_{r,s}^2 E_{r+1/2}^{(P)} = k_{r+1,s}^2 E_{r+1/2,s}^{(R)} \quad \text{(A2}b\text{)}$$

At these interfaces, $\partial E_x/\partial x$ satisfied the continuity conditions

$$(\partial E_x/\partial x)_{r-1/2,s}^{(L)} = (\partial E_x/\partial x)_{r-1/2,s}^{(P)} \quad \text{(A3}a\text{)}$$

$$(\partial E_x/\partial x)_{r+1/2,s}^{(P)} = (\partial E_x/\partial x)_{r+1/2,s}^{(R)} \quad \text{(A3}b\text{)}$$

It is now supposed that

(*a*) field value $E_{r,s}$ in dell *P* 'sees' a spurious field value $E_{r+1,s}^*$ in cell *R*, and

(*b*) field value $E_{r+1,s}$ in cell *R* 'sees' a spurious field value $E_{r,s}^*$ in cell *P*

By constructing the Taylor series

$$E_{r+1,s} = \sum_{m=0}^{\infty} (h_x/2)^m (\partial^m E_x/\partial x^m)_{r+1/2,s}^{(R)}$$

$$E_{r,s}^* = \sum_{m=0}^{\infty} (-h_x/2)^m (\partial^m E_x/\partial x^m)_{r+1/2,s}^{(R)}$$

$$E_{r+1,s}^* = \sum_{m=0}^{\infty} (h_x/2)^m (\partial^m E_x/\partial x^{m(P)}_{r+1/2,s}$$

$$E_{r,s} = \sum_{m=0}^{\infty} (-h_x/2)^m (\partial^m E_x/\partial x^m)_{r+1/2,s}^{(P)}$$

we find that

$$E_{r+1/2,s}^{(R)} = (E_{r+1,s} + E_{r,s}^*)/2 + 0(h_x^2) \quad \text{(A4}a\text{)}$$

$$h_x(\partial E_x/\partial x)_{r+1/2,s}^{(R)} = (E_{r+1,s} - E_{r,s}^*) + 0(h_x^2) \quad \text{(A4}b\text{)}$$

$$E_{r+1/2,s}^{(P)} = (E_{r+1,s}^* + E_{r,s})/2 + 0(h_x^2) \quad \text{(A5}a\text{)}$$

$$h_x(\partial E_x/\partial x)_{r+1/2,s}^{(P)} = (E_{r+1,s}^* - E_{r,s}) + 0(h_x^2) \quad \text{(A5}b\text{)}$$

By substituting (A4*a*) and (A5*a*) into (A2*b*), and (A4*b*) together with (A5*b*) into (*A*3*b*) we obtain

$$E_{r+1,s}^* = 2K_{r+1,s}^{(R)} E_{r+1,s} + [K_{r+1,s}^{(R)} - K_{r,s}^{(RP)}]E_{r,s} \quad \text{(A6)}$$

in which

$$K_{r+1,s}^{(R)} = k_{r+1,s}^2/(k_{r,s}^2 + k_{r+1,s}^2) \quad \text{(A7}a\text{)}$$

$$K_{r,s}^{(RP)} = k_{r,s}/(k_{r,s}^2 + k_{r+1,s}^2) \quad \text{(A7}b\text{)}$$

It is next supposed that

(*c*) field value $E_{r,s}$ in cell *P* 'sees' a spurious field value $E_{r-1,s}^{**}$ in cell L, and

(*d*) field value $E_{r-1,s}$ in cell L 'sees' a spurious field value $E_{r,s}^{**}$ in cell P.

Then a similar analysis to that given above causes eqns. A2*a* and A3*a* to yield

$$E_{r-1,s}^{**} = 2K_{r-1,s}^{(L)} E_{r-1,s} + [K_{r-1,s}^{(L)} - K_{r,s}^{(LP)}]E_{r,s} \quad \text{(A8)}$$

where

$$K_{r,s}^{(LP)} = k_{r,s}^a/(k_{r-1,s}^2 + k_{r,s}^2) \quad \text{(A9}a\text{)}$$

$$K_{r-1,s}^{(L)} = k_{r-1,s}^2/(k_{r-1,s}^2 + k_{r,s}^2) \quad \text{(A9}b\text{)}$$

We can now form the approximations

$$h_x^2(\partial^2 E_x/\partial x^2)_{r,s}^{(P)} \approx E_{r-1,s}^{**} - 2E_{r,s} + E_{r+1,s}^* = 2K_{r-1,s}^{(L)} E_{r-1,s} - [2 + (K_{r,s}^{(LP)} - K_{r-1,s}^{(L)}) + (K_{r,s}^{(RP)} - K_{r+1,s}^{(R)})]E_{r,s} + 2K_{r+1,s}^{(R)} E_{r+1,s} \quad \text{(A10}a\text{)}$$

$$h_y^2(\partial^2 E_x/\partial y^2)_{r,s}^{(P)} \approx E_{r,s-1} - 2E_{r,s} + E_{r,s+1} \quad \text{(A10}b\text{)}$$

which may be substituted into eqn. 13 to yield a five-point difference scheme which reduces to the usual form when cells L, P, and R have the same refractive index (i.e. when $k_{r-1,s} = k_{r,s} = k_{r+1,s}$). The new scheme leads to the algebraic eigenvalue equation (eqn. 14).

8.3 Quasi-TM modes

At the interface between cells B and P, the field component E_y satisfies the conditions

$$k_{r,s-1}^2 E_{r,s-1/2}^{(B)} = k_{r,s}^2 E_{r,s-1/2}^{(P)} \quad \text{(A11}a\text{)}$$

$$(\partial E_y/\partial y)_{r,s-1/2}^{(B)} = (\partial E_y/\partial y)_{r,s-1/2}^{(P)} \quad \text{(A11}b\text{)}$$

whilst at the interface between cells P and A we have the relations

$$k_{r,s}^2 E_{r,s+1/2}^{(P)} = k_{r,s+1}^2 E_{r,s+1/2}^{(A)} \quad \text{(A12}a\text{)}$$

$$(\partial E_y/\partial y)_{r,s+1/2}^{(P)} = (\partial E_y/\partial y)_{r,s+1/2}^{(A)} \quad \text{(A12}b\text{)}$$

where $E_{r,s} = E_y(x_r, y_s)$, etc. Then an analysis smililar to that carried out for quasi-TE modes yields the aprroximations

$$h_y^2(\partial^2 E_y/\partial y^2)_{r,s}^{(P)} \approx 2K_{r,s-1}^{(B)} E_{r,s-1} - [2 + (K_{r,s}^{(BP)} - K_{r,s-1}^{(B)}) + (K_{r,s}^{(AP)} - K_{r,s+1}^{(A)})]E_{r,s} + 2K_{r,s+1}^{(A)} E_{r,s+1} \quad \text{(A13}a\text{)}$$

$$h_x^2(\partial^2 E_y/\partial x^2)_{r,s}^{(P)} \approx E_{r-1,s} - 2E_{r,s} + E_{r+1,s} \quad \text{(A13}b\text{)}$$

in which

$$K^{(A)}_{r,s+1} = k^2_{r,s+1}/(k^2_{r,s} + k^2_{r,s+1}) \quad \text{(A14}a\text{)}$$

$$K^{(AP)}_{r,s} = k^2_{r,s}/(k^2_{r,s} + k^2_{r,s+1}) \quad \text{(A14}b\text{)}$$

$$K^{(BP)}_{r,s} = k^2_{r,s}/(k^2_{r,s-1} + k^2_{r,s}) \quad \text{(A14}c\text{)}$$

$$K^{(B)}_{r,s-1} = k^2_{r,s-1}/(k^2_{r,s-1} + k^2_{r,s}) \quad \text{(A14}d\text{)}$$

The approximations (eqn. (A13)), may be substituted into eqn. 17 to yield a five-point difference scheme that leads to the algebraic eigenvalue equation (eqn. 18). The new scheme reduces to the usual form when cells A, P, and B have the same refractive index.